Int. J. Multiphase Flow Vol. 16, No. 5, pp. 853–865, 1990
Printed in Great Britain.

0301-9322/90 $3.00 + 0.00

COOLING OF A FALLING LIQUID FILM THROUGH INTERFACIAL HEAT AND MASS TRANSFER

Y. L. TSAY, T. F. LIN and W. M. YAN
Department of Mechanical Engineering, National Chiao Tung University, Hsinchu 30050, Taiwan, R.O.C.

(*Received* 3 *November* 1988; *in revised form* 1 *March* 1990)

Abstract—A numerical analysis was carried out to study the detailed heat transfer characteristics for a falling liquid ethanol film by solving the respective governing equations for the liquid film and the induced gas flow together. Meanwhile an experimental system was set up to measure the overall cooling of the film. The measured data are in good agreement with the numerical predictions. It was observed that the cooling of the liquid film is mainly caused by the latent heat transfer connected with the vaporization of the liquid film. Significant liquid cooling results for the system with a high inlet liquid temperature or a low liquid flowrate.

Key Words: evaporation, heat and mass transfer

INTRODUCTION

Heat transfer through latent heat exchange connected with the vaporization of a liquid film, the so-called evaporative cooling, has been known for some time to be relatively effective in improving the performance of various heat transfer equipment. The purpose of this study is to enhance our understanding of the evaporative cooling process by performing a detailed analysis for interfacial heat and mass transfer in air over a falling liquid film combined with some experimental measurement.

Chun & Seban (1971) and Seban & Faghri (1976) experimentally and theoretically investigated the evaporation from a liquid water film to pure water vapor. In the theoretical studies they focused on the transport processes in the liquid film. In view of the complexity of the couplings between momentum, heat and mass transfer in the gas (air + vapor) flow and momentum and heat transfer in the liquid film through their common interface, other early studies focused on heat and mass transfer in the gas stream by assuming the liquid film to be extremely thin. Under this assumption the transport in the film can be replaced by the appropriate boundary conditions for the gas flow. This type of analysis was carried out for the buoyancy-induced heat and mass transfer over flat plates with different inclinations by Gill *et al.* (1965), Saville & Churchill (1970), Bottemanne (1971), Gebhart & Pera (1971) and Chen & Yuh (1979) and inside a circular pipe by Chang *et al.* (1986). A similar analysis was presented by Chandra & Savery (1974) and Chandra (1975) for an upward forced air flow over a free falling isopropyl alcohol film by the integral method. In their theoretical work the measured temperature and concentration distributions along the gas–liquid interface were used to specify the inhomogeneous boundary conditions required for solving the energy and species diffusion equations for the air–vapor flow. In addition, the laminar and turbulent forced convection boundary layer flow of gas over a vaporizing liquid film on a flat plate was numerically investigated by Schröppel & Thiele (1983) with the same assumption. Similar studies were conducted by Chow & Chung (1983a, b) for laminar and turbulent air flows of various humidity and superheated steam over a liquid water film. Recently, the evaporation rates of water were measured by Haji & Chow (1988) and the measured data agree well with the predicted values from Chow & Chung (1983b) if the heat loss from the water pan is accounted for.

Detailed analysis to include the transport processes in the liquid film were carried out recently. Conservation equations for the gas stream and liquid film were simultaneously solved for turbulent gas flow over a cocurrent liquid flow by Shembharkar & Pai (1986) and Baumann & Thiele (1986). In these studies the temperature distributions across the film were assumed to be linear.

A schematic diagram of the physical system to be investigated is shown in figure 1. A large vertical plate surrounded by still air at temperature T_∞ and ethanol vapor concentration $w_{v,\infty}$ is wetted by a thin, free falling liquid ethanol film fed at temperature $T_{L,in}$ and flowrate $\dot{m}_{L,in}$. The selection of ethanol for the liquid film is simply due to its strong volatility. The plate is well-insulated. As the liquid ethanol flows down over the plate, it drags the air adjacent to the film downwards through the viscous shearing effect at the liquid–gas interface. Apparently, this shear-induced flow would result in heat and mass transfer between the film and the gas flow. This heat and mass transfer process may be augmented or retarded by the buoyancy forces of thermal and mass diffusion, depending on the directions of the buoyancy forces, due to the differences in temperature and concentration between the interface and ambient. When $T_{L,in}$ is not much higher than T_∞, the gas flow induced by the combined action of the shear and buoyancy forces would move downwards.

In this study we performed a detailed numerical analysis by simultaneously solving the conservation equations for various transport processes in the liquid film and gas stream with the rigorous treatment of the interfacial matching conditions. Attention was particularly focused on the latent heat transfer associated with the film vaporization and the cooling of the film. To complement the numerical analysis, an experimental system was established to measure the cooling of the liquid film.

ANALYSIS

Heat and mass transfer processes in the liquid film and gas flow can be described in detail by the appropriate governing equations and interfacial conditions.

(A) Basic equations for the liquid film

Since only low liquid flowrate is considered here, the inertia terms in the momentum equation are small compared with the body force term and hence can be neglected. Furthermore, for the thin liquid film the longitudinal gradients of velocity and temperature are much smaller than those in the transverse direction. With these simplifications steady laminar momentum and heat transfer in the liquid film can be described by the following equations:

x-momentum equation,

$$0 = \frac{\partial}{\partial y}\left(\mu_L \frac{\partial u_L}{\partial y}\right) + \rho_L g; \qquad [1]$$

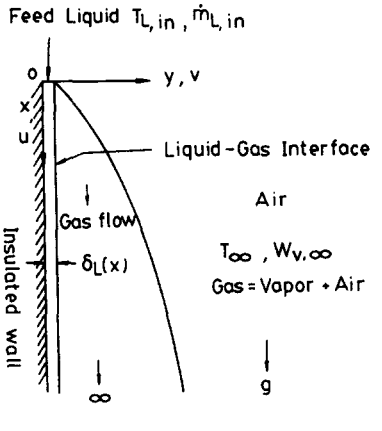

Figure 1. Schematic diagram of the physical system.

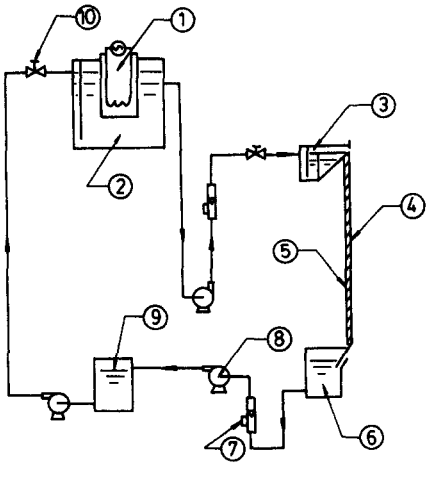

Figure 2. Schematic diagram of experimental apparatus: 1, electric heater; 2, liquid reservoir; 3, feed tank; 4, steel plate (test section); 5, balsa wood; 6, liquid collector; 7, flowmeter; 8, pump; 9, liquid collector; 10, valve.

and

energy equation,

$$\rho_L c_{pL} u_L \frac{\partial T_L}{\partial x} = \frac{\partial}{\partial y}\left(\lambda_L \frac{\partial T_L}{\partial y}\right). \quad [2]$$

(B) Basic equations for gas flow

As mentioned above, the induced gas flow moves downwards when $T_{L,in}$ is not much higher than T_∞. Steady laminar heat and mass transfer in the gas flow driven by the combined action of the interfacial shear force and the buoyancy forces of thermal and mass diffusion can be explored, with the boundary layer approximations, by the basic equations as:

continuity equation,

$$\frac{\partial}{\partial x}(\rho_G u_G) + \frac{\partial}{\partial y}(\rho_G v_G) = 0; \quad [3]$$

x-momentum equation,

$$\rho_G\left(u_G \frac{\partial u_G}{\partial x} + v_G \frac{\partial u_G}{\partial y}\right) = \frac{\partial}{\partial y}\left(\mu_G \frac{\partial u_G}{\partial y}\right) + (\rho_G - \rho_\infty)g; \quad [4]$$

energy equation

$$\rho_G c_{pG}\left(u_G \frac{\partial T_G}{\partial x} + v_G \frac{\partial T_G}{\partial y}\right) = \frac{\partial}{\partial y}\left(\lambda_G \frac{\partial T_G}{\partial y}\right) + \rho_G D(c_{pv} - c_{pa}) \frac{\partial T_G}{\partial y}\frac{\partial w_v}{\partial y}; \quad [5]$$

and

species diffusion equation of ethanol vapor,

$$\rho_G\left(u_G \frac{\partial w_v}{\partial x} + v_G \frac{\partial w_v}{\partial y}\right) = \frac{\partial}{\partial y}\left(\rho_G D \frac{\partial w_v}{\partial y}\right). \quad [6]$$

In the above equations ρ, u, v, T, w_v, μ, λ and D, respectively, stand for the density, longitudinal velocity, transverse velocity, temperature, mass fraction of ethanol vapor, dynamic viscosity, conductivity and mass diffusivity; c_{pL}, c_{pv} and c_{pa} are the specific heat of ethanol liquid, ethanol vapor and air, respectively, and g is the gravitational acceleration. The subscripts L and G denote the liquid and gas (vapor + air) phases, and ∞ is the ambient value.

(C) Boundary and interfacial conditions

The boundary conditions are:

at $x = 0$, $T_L = T_{L,in}$, $T_G = T_\infty$, $u_G = v_G = 0$, $w_v = w_{v,\infty}$; [7a]

at $y = 0$, $u_L = 0$, $\frac{\partial T_L}{\partial y} = 0$; [7b]

and

at $y \to \infty$, $u_G = 0$, $T_G = T_\infty$, $w_v = w_{v,\infty}$. [7c]

The matching conditions at the liquid–gas interface, $y = \delta_L(x)$, are given as:

1. Continuity of velocity, temperature and shear stress,

$$u_{L,i} = u_{G,i}, \quad T_{L,i} = T_{G,i}, \quad \left(\mu_L \frac{\partial u_L}{\partial y}\right)_i = \left(\mu_G \frac{\partial u_G}{\partial y}\right)_i, \quad [8]$$

where the subscript i denotes the interface.

2. Transverse velocity of gas is deduced by assuming the interface is semi-permeable—i.e. the solubility of air in liquid ethanol is negligibly small and air is stationary at the interface,

$$v_{G,i} = -\left(\frac{D}{1 - w_v}\frac{\partial w_v}{\partial y}\right)_i. \quad [9]$$

3. Assuming the interface to be at thermodynamic equilibrium and the air–ethanol vapor mixture as an ideal gas mixture, the mass fraction of the ethanol vapor can be calculated by, as in Chang *et al.* (1986),

$$w_{v,i} = \frac{M_v P_{v,i}}{M_a (P_\infty - P_{v,i}) + M_v P_{v,i}}, \quad [10]$$

where M_v and M_a represent the molecular weights of the ethanol vapor and air, respectively. $P_{v,i}$ is the vapor pressure of ethanol vapor at the interfacial temperature.

4. Energy balance at the interface,

$$-\left(\lambda_L \frac{\partial T_L}{\partial y}\right)_i = -\left(\lambda_G \frac{\partial T_G}{\partial y}\right)_i + m''_{v,i} \cdot h_{LG}, \quad [11]$$

here h_{LG} is the latent heat of vaporization. The evaporating flux of the ethanol vapor $m''_{v,i}$ is evaluated by the equation

$$m''_{v,i} = -\left(\frac{\rho_G D}{1 - w_v} \cdot \frac{\partial w_v}{\partial y}\right)_i. \quad [12]$$

It should be pointed out here that the wave motion of the liquid–gas interface is relatively complex and no systematic study of the wave characteristics for the liquid ethanol film exists in the literature. In the present analysis the effects of the wave motion on the interfacial transport processes are ignored.

The variations of the thermophysical properties with temperature and mixture composition are important for the liquid film and the gas mixture, and are accounted for in the computation. Complete details on the evaluation of these properties are given in the appendix.

SOLUTION METHOD

Since the flows governed by [1]–[6] are parabolic in x, the finite-difference solution for these equations can be marched in the downstream direction. A fully implicit numerical scheme, in which the longitudinal convection terms are approximated by the upstream difference and the transverse convection and diffusion terms by the central difference, is employed to transform the governing equations into finite-difference equations. Each system of the finite-difference equations forms a tridiagonal matrix equation which can be efficiently solved by the Thomas algorithm, described by Anderson *et al.* (1984). For a given flow and thermal condition a brief outline of the solution procedures is described as follows:

(1) For a longitudinal location x_j guess a film thickness $\delta_{L,j}$.
(2) Solve the finite-difference forms of [1] and [4] simultaneously for u_L and u_G.
(3) Numerically integrate [3] to find v_G.
(4) Solve the finite-difference forms of [2] and [5] together for T_L and T_G.
(5) Solve the finite-difference form of [6] for w_v.
(6) Check if the relative error between two consecutive iterations $n-1$ and n is small enough, i.e. $|\phi^n - \phi^{n-1}|/|\phi^n|_{max} < 10^{-3}$ for all nodal points where ϕ represents the variables u_G, u_L, T_G, T_L or w_v. If not, repeat procedures (2)–(6).
(7) Check the mass conservation of the liquid ethanol film by examining the satisfaction of the inequality,

$$\left|\frac{(\dot{m}_{L,j-1} - \dot{m}_{L,j}) - (m''_{v,j} \cdot \Delta x_j)}{(\dot{m}_{L,j-1} - \dot{m}_{L,j})}\right| < 10^{-4}, \quad [13]$$

where the subscript j denotes the jth longitudinal grid point. The mass flowrate of the ethanol liquid is calculated by

$$\dot{m}_{L,j} = \int_0^{\delta_{L,j}} \rho_L \cdot u_L \, dy. \quad [14]$$

If [13] is not satisfied, guess a new film thickness and repeat procedures (2)–(7) for the current location. If yes, proceed to the next longitudinal location and apply procedures (1)–(7).

To account for the change in liquid film thickness $\delta_L(x)$ due to the film vaporization, the finite-difference computational grid used must comply with the variations of computation domains with x. This was accomplished by first locating the interface at every longitudinal location, and then dividing the film and gas regions in the y-direction into n_L and n_G points, respectively. Thus, the interface position was rigorously traced. This adjustment of the grid in the y-direction necessitates numerical interpolation when evaluating the convection terms. To further account for the drastic variations of velocity, temperature and concentration in the regions near the leading edge and interface, a nonuniform grid was chosen. The computation domain is taken to be 1 m in the x-direction and 0.05–0.06 m in the y-direction for various cases. The nonuniformity of the grid is described here in detail—$\Delta x_1 = 1.443 \times 10^{-3}$ m and $\Delta x_j = 1.005 \times \Delta x_{j-1}$; in the film, $\Delta y_1 = (1.27 \text{ to } 2.073) \times 10^{-5}$ m close to the plate and $\Delta y_k = 0.95 \times \Delta y_{k-1}$; in the gas flow, $\Delta y_1 = (1.461 \text{ to } 1.753) \times 10^{-4}$ m near the interface and $\Delta y_k = 1.005 \times \Delta y_{k-1}$. Here k is the kth transverse grid point.

During the program test several grid sizes were employed. A comparison of the results for the distributions of the interfacial temperature $T_{L,i}$, the interfacial sensible heat flux in the gas side, $q''_{G,i} = -(\lambda_G \partial T_G/\partial y)_i$, and the interfacial sensible heat flux in the liquid side, $q''_{L,i} = -(\lambda_L \partial T_L/\partial y)_i$, from these computations for a typical case is shown in table 1. It is noted that the differences in the results obtained using the 301 × 221 and 401 × 331 grids are always <2%. Accordingly, the 301 × 221 grid was used in all the subsequent computations.

DESCRIPTION OF EXPERIMENTAL APPARATUS

Depicted in figure 2 is the schematic arrangement of the experimental setup. The facility consists of a closed-loop liquid delivery system, a test section, a heating system and a data acquisition system with some related instruments. As shown in the figure, liquid ethanol falls down along a large vertical plate from a feed tank and is collected as it leaves the plate. The thickness of the liquid film at the inlet is controlled by the liquid level in the feed tank. The liquid in the collector is then pumped to a reservoir where it is heated by a preheater. To accurately control the liquid temperature in the reservoir, an automatic feedback heating system comprising a very sensible platinum rod, a temperature controller and a power regulator is used. The test section is made of a stainless-steel SS304 plate sheet, 1 m long × 30 cm wide × 1 mm thick. In order to support the plate sheet and insulate it, a balsa wood plate 1.5 cm thick is glued on the plate. It is worth noting that the spanwise uniformity of the liquid film thickness is important in maintaining all the transfer processes two-dimensional. To uniformly wet the surface of the steel plate, the plate surface is rubbed with emery paper.

Table 1. Comparison of $T_{L,i}$, $q''_{G,i}$ and $q''_{L,i}$ for various grid arrangements for case II

	x (m)	201 × 111 $n_x = 201$, $n_L = 11$, $n_G = 100$	301 × 221 $n_x = 301$, $n_L = 21$, $n_G = 200$	401 × 331 $n_x = 401$, $n_L = 31$, $n_G = 300$
$T_{L,i}$ (°C)	0.02	28.79	28.85	28.87
	0.10	28.03	28.09	28.10
	0.40	26.24	26.41	26.39
	1.0	24.25	24.50	24.37
$q''_{G,i}$ (W/m²)	0.02	10.21	9.92	9.73
	0.10	11.01	10.87	10.67
	0.40	13.95	13.64	13.66
	1.0	16.54	16.11	16.34
$q''_{L,i}$ (W/m²)	0.02	1037.26	1009.39	989.24
	0.10	431.63	423.74	428.62
	0.40	215.42	215.09	212.03
	1.0	126.78	128.22	127.33

Copper–constantan thermocouples were used to measure the plate temperatures. They were installed along the longitudinal centerline of the plate and spaced 50 or 100 mm apart. In addition, at three longitudinal locations thermocouples were fixed at three spanwise positions to check the spanwise uniformity of the liquid film temperature. Prior to installation the thermocouples were calibrated by a LAUDA compact low-temperature thermostat (type RKS20-D) with a YEW digital thermometer (type 2575). The overall accuracy of the thermocouples is believed to be well within 0.2°C. To maintain the smoothness of the testing surface, the thermocouples were glued, instead of being welded, to the back surface of the plate to prevent surface distortion resulting from the concentrated thermal stress during welding. For the purpose of estimating heat gain or loss from the test section through the balsa wood, a number of thermocouples were also glued to the outer surface of the wood.

The measured temperatures need to be corrected for the heat gain or loss. For the thin liquid film considered and the plate well-insulated, the plate temperature is relatively close to the film temperature at the same x-location. This becomes evident later when the results from the numerical computations are examined. A simple energy balance dictates that the measured temperatures can be corrected by the relation

$$T_{w,x} = T'_{w,x} - \int_0^x \frac{q''_{x,c}}{\dot{m}_L c_{pL}} dx, \qquad [15]$$

where $T'_{w,x}$ and $T_{w,x}$ are, respectively, the measured and corrected local plate temperatures $q''_{x,c}$ is the heat gain or loss through the wood, which is evaluated by the equation

$$q''_{x,c} = -\lambda_b \frac{\Delta T_b}{\delta_b}, \qquad [16]$$

here ΔT_b is the temperature difference across the wood plate, and δ_b and λ_b are the thickness and conductivity of the wood plate, respectively.

The flowrates of the liquid film were measured by variable-area-type flowmeters (M-type). All the flowmeters were calibrated by the static weighting procedure, described by Mattingly (1983), at several liquid temperatures to account for the property variations with temperature. The accuracy of the flowrate measurement is believed to be within 0.00987 kg/min.

RESULTS AND DISCUSSION

In the numerical study computations were performed for the cases specified in table 2. For the first three cases $T_{L,in} = T_\infty$ and the liquid film flowrate varies from 0.01 to 0.04 kg/m · s. $T_{L,in}$ is higher than T_∞ for cases IV–VI. In the following, results are presented to illustrate the effects of $T_{L,in}$ and $\dot{m}_{L,in}$ on the detailed heat and mass transfer processes in the liquid film and gas flow.

Cooling of the liquid film when $T_{L,in} = T_\infty$ for cases I–III is of considerable interest. As the liquid ethanol leaves the feed tank and falls down along the plate, it has the same temperature as the ambient air and hence no sensible heat transfer occurs. But note that the concentration of the ethanol vapor at the interface is higher than that in the ambient, mass diffusion of ethanol vapor takes place accordingly. This mass transfer process absorbs a significant amount of energy ($m''_{v,i} \cdot h_{LG}$) through latent heat transport, as evident from [11]. This amount of energy is supplied

Table 2. The datum conditions to be studied

Case	$T_{L,in}$ (°C)	$\dot{m}_{L,in}$ (kg/m · s)	T_∞ (°C)	$W_{v,\infty}$	$Re_{L,in}$	$\delta_{L,in}$ (m)
I	30	0.01	30	0	42.1	$1.67\ 10^{-4}$
II	30	0.02	30	0	84.2	$2.11\ 10^{-4}$
III	30	0.04	30	0	168.5	$2.66\ 10^{-4}$
IV	35	0.01	30	0	46.1	$1.63\ 10^{-4}$
V	35	0.02	30	0	92.2	$2.05\ 10^{-4}$
VI	35	0.04	30	0	184.4	$2.59\ 10^{-4}$

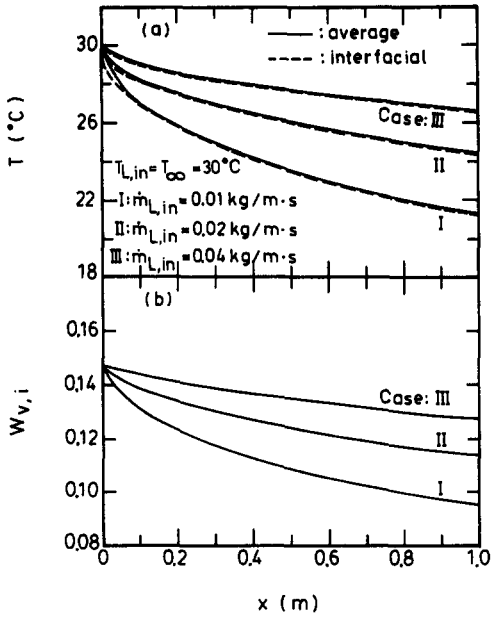

Figure 3. Distributions of liquid average temperature, interfacial temperature (a) and interfacial mass fraction of ethanol vapor (b).

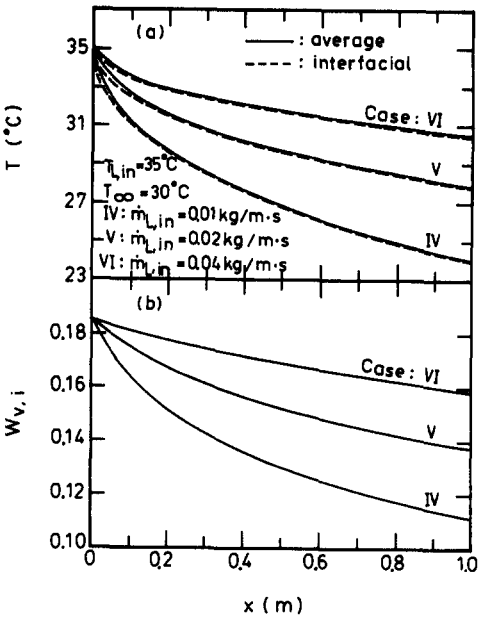

Figure 4. Distributions of liquid average temperature, interfacial temperature (a) and interfacial mass fraction of ethanol vapor (b).

by the liquid film and gas flow through the loss of sensible heat. Therefore, both the liquid and gas flow are gradually cooled. Apparently, the whole process is mainly driven by the mass transfer process. Figure 3 shows the predicted cooling of the liquid film for $T_{L,in} = T_\infty$ by plotting the x-variations of the average liquid film temperature. Also included in the figure are the distributions of the temperature and ethanol vapor concentration at the interface. The results in figure 3(a) clearly indicate that smaller liquid film cooling is experienced for a larger liquid film flowrate. This is readily understood by realizing that the total internal energy stored in the liquid is larger for a higher $\dot{m}_L$ and that a simple energy balance for the liquid film gives $\dot{m}_L c_{pL} \Delta T_{L,ave} = q''_{L,i}$. Hence for a larger $\dot{m}_L$, ΔT_L is smaller. Also noted in figure 3(a) is the relatively small temperature difference between $T_{L,ave}$ and $T_{L,i}$ for a given x, except in the region near the leading edge because the liquid film is rather thin. The predicted ethanol vapor concentration in figure 3(b) follows the same trend as the interface temperature, since thermodynamic equilibrium was assumed there.

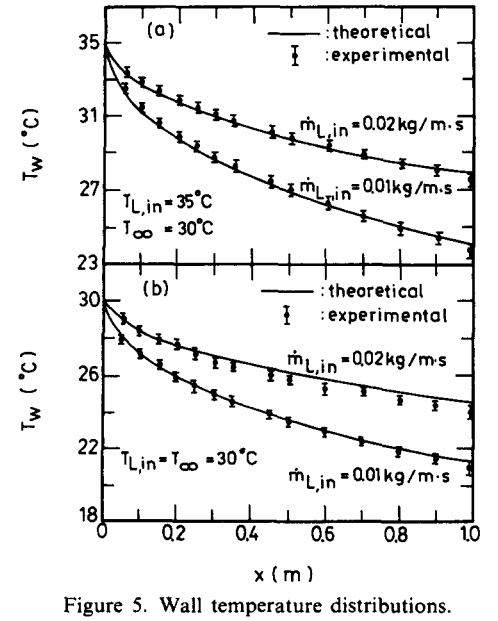

Figure 5. Wall temperature distributions.

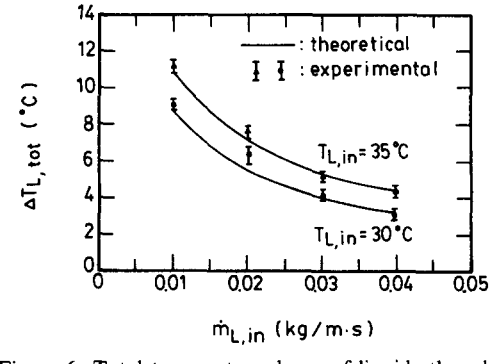

Figure 6. Total temperature drops of liquid ethanol.

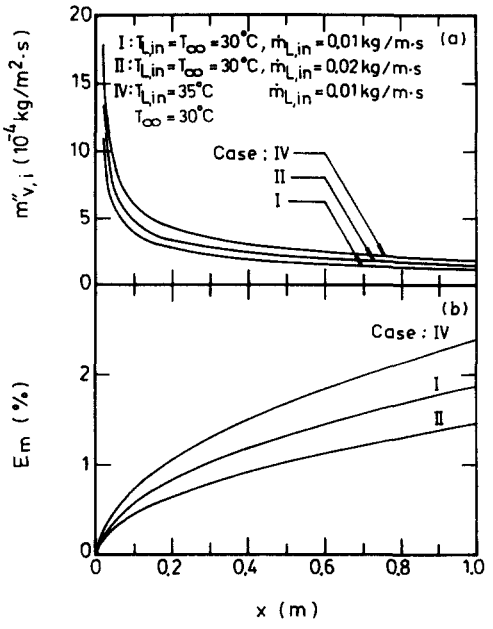

Figure 7. Distributions of the mass flux of ethanol vapor at the interface flowing into the gas stream (a) and relative flux of film vaporization (b).

A larger temperature drop in the liquid film is experienced when $T_{L,in}$ is increased to 35°C from the results given in figure 4(a). This is a direct consequence of the larger difference in ethanol vapor concentration between the interface and ambient for a higher $T_{L,i}$ [figure 4(b)] which, in turn, causes larger film vaporization and heat transfer.

The measured wall temperature distributions are compared with the predicted values in figure 5 for four different cases. Excellent agreement is noted, which lends strong support to the theoretical model employed in the computation. Good agreement is also observed in figure 6 between the measured and predicted total temperature drop of the liquid film, $\Delta T_{L,tot} = T_{L,in} - T_{L,out}$.

As noted above, heat and mass transfer in the system is dominated by the film vaporization. Figures 7(a, b), respectively, present the effects of $\dot{m}_{L,in}$ and $T_{L,in}$ on the absolute evaporative mass flux of ethanol vapor at the interface and the relative flux of film vaporization Em defined as

$$Em = \frac{\int_0^x m''_{v,i}\,dx}{\dot{m}_{L,in}}. \qquad [17]$$

For a given case, the evaporative flux decreases in the flow direction, which is in line with the decreases in the interface temperature $T_{L,i}$ and ethanol vapor concentration $w_{v,i}$ in figures 3 and 4.

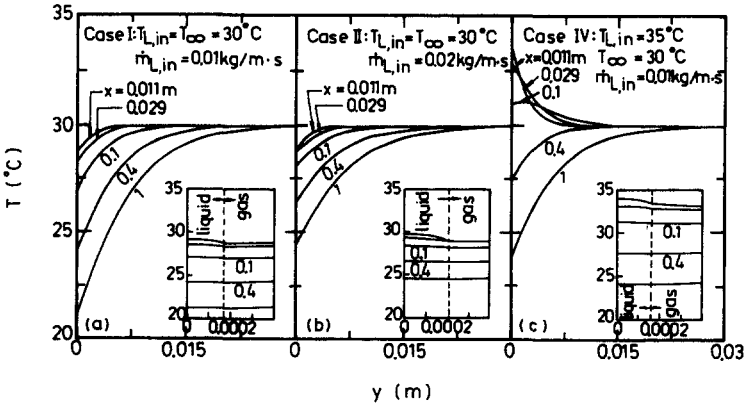

Figure 8. Temperature profiles of the liquid film and gas stream at various longitudinal locations.

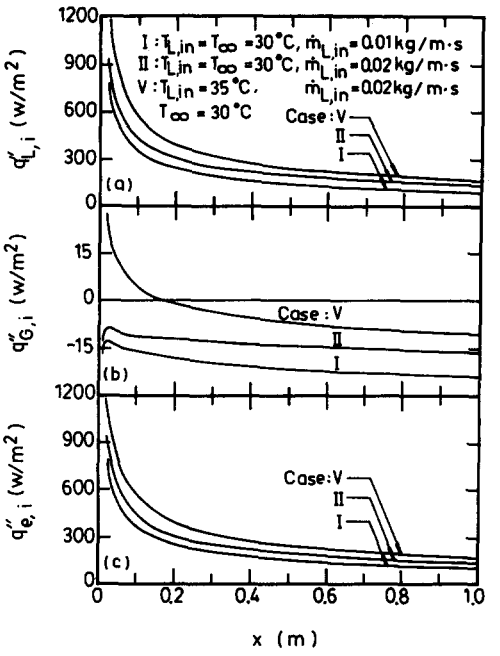

Figure 9. Local interfacial heat flux distributions.

While for a rise in the film flowrate or inlet temperature of the liquid film, stronger film vaporization results—simply owing to the associated increase in $T_{L,i}$ and $w_{v,i}$. The results for *Em* in figure 7(b) clearly show that the total amount of film vaporization is only about 2% of the film flowrate.

Detailed heat transfer characteristics in the flow can be illustrated by examining the developments of the temperature profile in figures 8(a–c). The inset plots in these figures are to provide a close look at the heat transfer process near the interface. For $T_{L,in} = T_\infty$, the results given in figures 8(a, b) indicate that the sensible heat transfer in the gas stream is toward the interface, so is the sensible heat transfer in the film. Obviously, heat transfer toward the interface is absorbed during the film vaporization process. For $T_{L,in} > T_\infty$, in figure 8(c), sensible heat transfer in the film is also toward the interface. But in the gas flow, sensible heat transfer is first from the interface to the ambient because $T_{L,i} > T_\infty$. The heat transfer direction reverses in the downstream as the liquid film is cooled to the degree that the gas mixture near the interface is at a higher temperature than that of the liquid film, as evident in the curves for $x = 0.1$, 0.4 and 1.0 m [figure 8(c)]. Also noted in these figures is the uniformity of the liquid temperature in the y-direction except near the leading edge, $x = 0.011$ and 0.029 m.

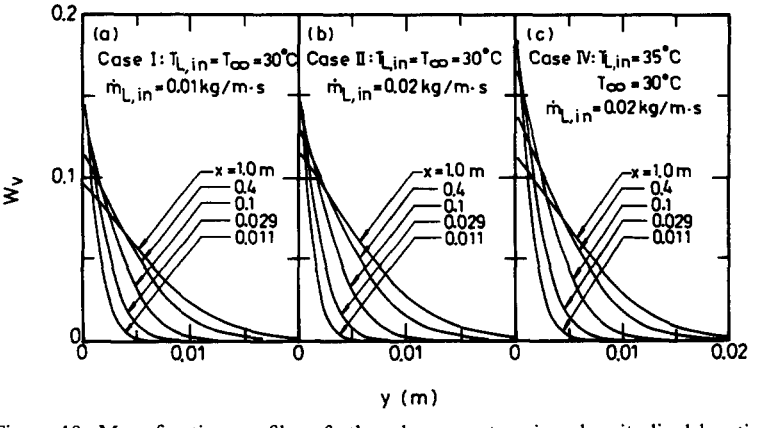

Figure 10. Mass fraction profiles of ethanol vapor at various longitudinal locations.

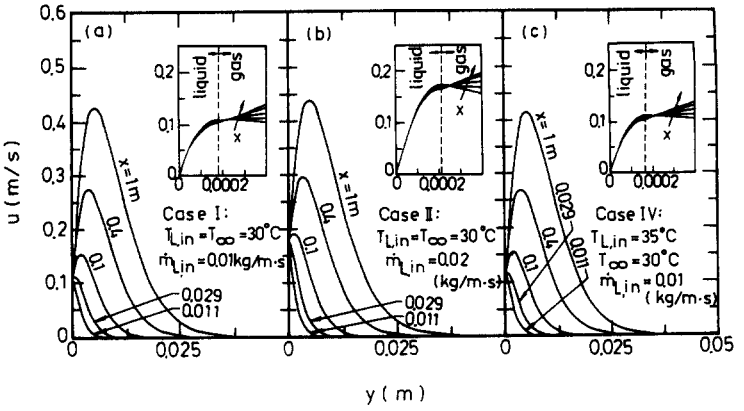

Figure 11. Velocity profiles of the liquid film and gas stream at various longitudinal locations.

Next, we examine the effects of $\dot{m}_{L,in}$ and $T_{L,in}$ on the interface energy balance, [11]. Figures 9(a–c) show the predicted distributions of the sensible heat fluxes in the liquid side $q''_{L,i}$ and in the gas side $q''_{G,i}$ and of the energy absorption by the film vaporization $q''_{e,i}=m''_{v,i}h_{LG}$. First, we note that $q''_{L,i}$ is much larger than $q''_{G,i}$ due to the simple fact that the film is relatively thin and the thermal conductivity of liquid ethanol is much higher than that of gas. This indicates that the energy required for the film vaporization is mainly provided by the sensible heat transfer from the liquid film and effective cooling of the liquid film thus results.

Also noted in figure 9(a) is that $q''_{L,i}$ is larger for the cases with a higher $T_{L,in}$ or $\dot{m}_{L,in}$, which is brought about by the larger film vaporization associated with these cases, as just discussed. It is of interest to notice that in figure 9(b) the magnitude $q''_{G,i}$ increases in the x-direction except in the region near the leading edge. The result is a direct consequence of the continuing drop in the interface temperature in the x-direction so that the temperature difference, $(T_{L,i}-T_\infty)$, becomes larger. For case V, the change in the sensible heat transfer direction is clearly shown.

For all cases studied the latent heat transfer connected with the film vaporization is always positive, indicating the occurrence of interfacial vaporization instead of condensation. Note also that the latent heat transfer is relatively effective.

The concentration distributions of the ethanol vapor in the gas stream given in figure 10 show that more ethanol vapor exists in the gas flow when $T_{L,in}$ or $\dot{m}_{L,in}$ is higher. The results is in line with the above discussion that at higher $T_{L,in}$ or $\dot{m}_{L,in}$ larger vaporization occurs at the interface. It is also noted in figure 10 that the mass fraction of ethanol vapor near the interface decreases in the x-direction, obviously resulting from the drop in the interface temperature in that direction.

The velocity fields in the liquid film and gas stream, simultaneously influenced by the interfacial shear force and the combined buoyancy forces of thermal and mass diffusion, are illustrated in figure 11. The inset plots in the figure give the velocity profiles near the interface. The results indicate that the gas velocity is only slightly influenced by the change in the liquid film flowrate or liquid inlet temperature. For an increase in $\dot{m}_{L,in}$ the velocity at the interface is higher. While for a higher $T_{L,in}$ insignificant change in the flow field results since the increased upward thermal buoyancy is offset by the larger downward concentration buoyancy due to the higher interface vapor concentration at higher $T_{L,i}$. It should be pointed out that the appearance of the velocity peaks in the gas flow apparently signifies the important action of the buoyancy forces, otherwise no velocity peaks would exist. A close examination of the inset plots reveals that the liquid velocity slightly decreases in the flow direction. The result is caused by the increase in the liquid viscosity when the liquid film is cooled.

CONCLUDING REMARKS

A numerical analysis has been carried out to explore the detailed heat transfer characteristics for a falling liquid film cooled through interfacial heat and mass transfer by solving the respective governing equations for the liquid film and the induced flow coupled together by the interfacial

matching conditions. The predicted overall cooling of the liquid film compares favorably with the measured data performed in the present study. The major results are briefly summarized in the following:

(1) The cooling of the liquid film is mainly caused by the latent heat transfer connected with the vaporization of the liquid film.
(2) The liquid film experiences a larger temperature drop for a rise in the inlet temperature of the film. While the reverse is true for an increase in the flowrate of the film.
(3) When $T_{L,in} = T_\infty$, the sensible heat transfer in the film and gas flow is initiated by the latent heat transfer due to the film vaporization.

It has been realized during the course of the study that when $T_{L,in}$ is much higher than T_∞, and the upward thermal buoyancy force may overcome the downward interfacial shear force and solutal buoyancy force, flow reversal then results in certain parts of the flow. If a liquid water film is considered, flow reversal is prone to occur since the mass diffusion buoyancy force is always upward. Under these situations, a more complicated elliptic flow analysis must be performed.

Acknowledgement—The financial support of this study by the Engineering Division of the National Science Council, Taiwan, R.O.C., through Contract NSC77-0401-E009-10 is greatly appreciated.

REFERENCES

ANDERSON, D. A., TANNEHILL, J. C. & PLETCHER, R. H. 1984 *Computational Fluid Mechanics and Heat Transfer*, Chap. 7. Hemisphere/McGraw-Hill, New York.

BAUMANN, W. W. & THIELE, F. 1986 Heat and mass transfer in two-component film evaporation in a vertical tube. *Proc. 8th Int. Heat Transfer Conf.* **4,** 1843–1848.

BIRD, R. B., STEWART, W. E. & LIGHTFOOT, E. N. 1960 *Transport Phenomena.* Wiley, New York.

BOTTEMANNE, F. A. 1971 Theoretical solution of simultaneous heat and mass transfer by free convection about a vertical flat plate. *Appl. scient. Res.* **25,** 137–149.

CHANDRA, V. 1975 Mass, momentum and heat transfer from a falling film to a countercurrent air stream. Ph.D Thesis, Drexel Univ., Philadelphia, Pa.

CHANDRA, V. & SAVERY, C. W. 1974 Forced convective heat and mass transfer from a falling film to a laminar external boundary layer. *Int. J. Heat Mass Transfer* **17,** 1549–1557.

CHANG, C. J., LIN, T. F. & YAN, W. M. 1986 Natural convection flows in a vertical, open tube resulting from combined buoyancy effects of thermal and mass diffusion. *Int. J. Heat Mass Transfer* **29,** 1543–1552.

CHEN, T. S. & YUH, C. F. 1979 Combined heat and mass transfer in natural convection on inclined surfaces. *Numer. Heat Transfer* **2,** 233–250.

CHOW, L. C. & CHUNG, J. N. 1983a Evaporation of water into a laminar stream of air and superheated steam. *Int. J. Heat Mass Transfer* **26,** 373–380.

CHOW, L. C. & CHUNG, J. N.1983b Water evaporation into a turbulent stream of air, humid air or superheated steam. In *Proc. 21st ASME/AICHE National Heat Transfer Conf.*, Seattle, Wash., ASME Paper No. 83-HT-2.

CHUN, K. R. & SEBAN, R. A. 1971 Heat transfer to evaporating liquid film. *ASME Jl Heat Transfer* **93,** 391–396.

FUJII, T., KATO, Y. & MIHARA, K. 1977 Expressions of transport and thermodynamic properties of air, steam and water. Sei San Ka Gaku Ken Kyu Jo, Report No. 66, Kyu Shu Dai Gaku, Kyu Shu, Japan.

GEBHART, B. & PERA, L. 1971 The nature of vertical natural convection flows resulting from the combined buoyancy effects of thermal and mass diffusion. *Int. J. Heat Mass Transfer* **14,** 2025–2050.

GILL, W. N., CASAL, E. D. & ZEH, D. W. 1965 Binary diffusion and heat transfer in laminar free convection boundary layers on a vertical plate. *Int. J. Heat Mass Transfer* **8,** 1135–1151.

HAJI, M. & CHOW, L. C. 1988 Experimental measurement of water evaporation rates into air and superheated steam. *ASME Jl Heat Transfer* **110,** 237–242.

MATTINGLY, G. E. 1983 *Volume Flow Measurements, in Fluid Mechanics Measurements*, Chap. 6 (Edited by GOLDSTEIN, R. J.). Hemisphere, Washington, D.C.

SAVILLE, D. A. & CHURCHILL, S. W. 1970 Simultaneous heat and mass transfer in free convection boundary layers. *AIChE Jl* **16,** 268–273.

SCHRÖPPEL, J. & THIELE, F. 1983 On the calculation of momentum, heat and mass transfer in laminar and turbulent boundary layer flows along a vaporizing liquid film. *Numer. Heat Transfer* **6,** 475–496.

SEBAN, R. A. & FAGHRI, A. 1976 Evaporation and heating with turbulent falling liquid films. *ASME Jl Heat Transfer* **98,** 315–318.

SHEMBHARKAR, T. R. & PAI, B. R. 1986 Prediction of film cooling with a liquid coolant. *Int. J. Heat Mass Transfer* **29,** 899–908.

YANO, T. & UCHIDA, H. 1983 Thermophysical properties of fluids. In *JSME Data Book*. JSME, Tokyo.

APPENDIX

Evaluation of Thermophysical Properties

The properties of air, ethanol vapor, air–ethanol vapor mixture and ethanol liquid are calculated by the following formulas:

air, described by Fujii *et al.* (1977),

$$\mu_a = \frac{1.4888 \times 10^{-6} \cdot T^{1.5}}{(188 + T)} \quad (\text{kg/m} \cdot \text{s}), \tag{A.1}$$

$$\lambda_a = \frac{1.195 \times 10^{-3} \cdot T^{1.6}}{(118 + T)} \quad (\text{W/m} \cdot \text{K}) \tag{A.2}$$

and

$$c_{pa} = (1 + 2.5 \times 10^{-10} \cdot T^3) \times 10^3 \quad (\text{J/kg} \cdot \text{K}); \tag{A.3}$$

ethanol vapor, described by Yano & Uchida (1983),

$$\log_{10} P_v = -10.967 - \frac{2212.6}{T} + 10.298 \log_{10} T - 2.1061 \times 10^{-2} T + 1.0748 \times 10^{-5} T^2 \quad (\text{mmHg}), \tag{A.4}$$

$$\mu_v = (1.396 + 0.2848T + 1.241 \times 10^{-5} T^2) \times 10^{-7} \quad (\text{kg/m} \cdot \text{s}), \tag{A.5}$$

$$\lambda_v = (-18.62 + 9.95 \times 10^{-2} T + 2.9 \times 10^{-4} T^2 - 1.238 \times 10^{-7} T^3) \times 4.18605 \times 10^{-4} \quad (\text{W/m} \cdot \text{K}) \tag{A.6}$$

and

$$c_{pv} = (0.239 + 6.23 \times 10^{-2} T - 3.806 \times 10^{-5} T^2 + 9.47 \times 10^{-9} T^3) \times 90.8628 \quad (\text{J/kg} \cdot \text{K}); \tag{A.7}$$

air–ethanol vapor mixture, described by Bird *et al.* (1960),

$$\mu_G = \frac{\mu_a}{1 + \left(\frac{x_v}{x_a}\right)\phi_{av}} + \frac{\mu_v}{1 + \left(\frac{x_a}{x_v}\right)\phi_{va}} \quad (\text{kg/m} \cdot \text{s}), \tag{A.8}$$

where x_a and x_v are the mole fractions of air and ethanol vapor, respectively, and

$$\phi_{i,j} = \frac{\left[1 + \left(\frac{\mu_i}{\mu_j}\right)^{0.5} \left(\frac{M_j}{M_i}\right)^{0.25}\right]^2}{\left[8\left(1 + \frac{M_i}{M_j}\right)\right]^{0.5}} \tag{A.9}$$

and

$$\lambda_G = \frac{\lambda_a}{1 + \left(\frac{x_v}{x_a}\right)\phi_{av}} + \frac{\lambda_v}{1 + \left(\frac{x_a}{x_v}\right)\phi_{va}} \quad (\mathrm{w/m \cdot K}), \qquad [A.10]$$

where ϕ_{av} and ϕ_{va} are identical to those that appeared in the viscosity equation [A.8]; mass diffusivity, described by Bird *et al.* (1960),

$$D = 1.8583 \times 10^{-7} \frac{\sqrt{T^3\left(\frac{1}{M_v} + \frac{1}{M_a}\right)}}{P\sigma_{va}^2 \Omega} \quad (\mathrm{m^2/s}), \qquad [A.11]$$

$$\Omega = \frac{A}{\bar{T}} + \frac{C}{\exp(D\bar{T})} + \frac{E}{\exp(F\bar{T})} + \frac{G}{\exp(H\bar{T})}, \qquad [A.12]$$

$$\bar{T} = \frac{T}{168.82}, \quad A = 1.06036, \quad B = 0.1561, \quad C = 0.193, \quad D = 0.47635,$$

$$E = 1.03587, \quad F = 1.52996, \quad G = 1.76474, \quad H = 3.89411, \quad \sigma_{va} = 4.1205;$$

and

ethanol liquid, described by Yano & Uchida (1983),

$$\rho_L = 290.3 \times 0.2765^{-[1-(T/516.26)]^{0.2857}} \quad (\mathrm{kg/m^3}) \qquad [A.13]$$

and

$$\mu_L = 10^A \times 10^{-3} \quad (\mathrm{kg/m \cdot s}), \qquad [A.14]$$

where

$$A = -2.697 + \frac{700.9}{T} + 2.682 \times 10^{-3}T - 4.917 \times 10^{-6}T^2, \qquad [A.15]$$

$$C_{pL} = 4.18605 \times 10^3 \times (-0.3499 + 9.559 \times 10^{-3}T - 3.786 \times 10^{-5}T^2 + 5.459 \times 10^{-8}T^3) \quad (\mathrm{J/kg \cdot K}) \qquad [A.16]$$

and

$$h_{LG} = 8.4809 \times 10^5 \left[\frac{(512.56 - T)}{161.1}\right]^{0.4} \quad (\mathrm{J/kg}). \qquad [A.17]$$